

# On the dynamics and morphology of extensive tidal mudflats: Integrating remote sensing data with an inundation model of Cook Inlet, Alaska

Tal Ezer · Hua Liu

Received: 13 April 2010 / Accepted: 11 July 2010 / Published online: 23 July 2010  
© Springer-Verlag 2010

**Abstract** A new method of integrating satellite remote sensing data and inundation models allows the mapping of extensive tidal mudflats in a sub-Arctic estuary, Cook Inlet (CI), Alaska. The rapid movement of the shorelines in CI due to the large tides (~10 m range) is detected from a series of Landsat imagery taken at different tidal stages, whereas GIS tools are used to identify the water coverage in each satellite image and to extract the coordinates of the shoreline. Then, water level along the shoreline for each satellite image is calculated from the observed water level at Anchorage and the statistics of an inundation model. Several applications of the analysis are demonstrated: 1. studying the dynamics of a tidal bore and the flood/ebb processes, 2. identifying climatic changes in mudflats morphology, and 3. mapping previously unobserved mudflat topographies in order to improve inundation models. The method can be used in other regions to evaluate models and improve predictions of catastrophic floods such as those associated with hurricane storm surges and tsunamis.

**Keywords** Remote sensing · Ocean modeling · Alaska · Tides

---

Responsible Editor: Joerg-Olaf Wolff

---

T. Ezer (✉)  
Center for Coastal Physical Oceanography,  
Old Dominion University,  
4111 Monarch Way,  
Norfolk, VA 23508, USA  
e-mail: tezer@odu.edu

H. Liu  
Department of Political Science and Geography,  
Old Dominion University,  
Norfolk, VA 23529, USA

## 1 Introduction

Coastal regions are continuously being changed by man-made shore developments and natural impacts like vegetation changes, land and sea sediment movements, sea-level rise, and in some cases by catastrophic events such as tropical storm surges or tsunamis. It is thus critical to have flood prediction models that can simulate and possibly predict the impact of catastrophic events such as the flooding of New Orleans in 2005 by Katrina (Travis 2005) or the 2004 tsunami in the Indian Ocean (Kowalik et al. 2006). Flood (or inundation) numerical models require, in addition to atmospheric forcing, detailed coastal and land topography data. However, in many coastal regions, detailed high-resolution topographic data are either not available, or the land is being changed by human development or natural climatic impacts. Very high-resolution (~1 m) flood-inundation maps from airborne LiDAR data can be very useful (Bales et al. 2007; Zhou 2009), but these data are costly and not easily available everywhere on the globe. Therefore, this study aims to develop new methodologies that use publicly available satellite remote sensing data to study the dynamics and morphology of flood zones that are otherwise unobserved by direct measurements (for example, mudflats are often too dangerous for making shipboard ocean measurements). Satellite imagery as well as LiDAR and aerial photography are often used qualitatively for catastrophic flooding to show “before and after” pictures, however, in this study we would like to demonstrate a more quantitative use of satellite remote sensing data to actually map changing coastlines and morphology and potentially incorporate the new data in flood prediction models.

The rare occurrence and unpredictable nature of catastrophic events make it difficult to study the impact of

extreme flooding events. Alternatively, one may use locations where flooding processes occur naturally as a test-bed laboratory to evaluate flood prediction and observation techniques. One such place is Cook Inlet (CI), Alaska, a sub-Arctic estuary with extremely large tides of  $\sim 10$  m range and energetic tidal bores and rip currents (Oey et al. 2007; Fig. 1). CI is subject to coastal population development (about half of Alaska's population lives in Anchorage and around Cook Inlet) and sensitive ecosystems which might be affected by climate change. For example, the (recently declared "Endangered Species") population of CI's beluga whales is declining, and may be affected by climate change and coastal development (Ezer et al. 2008). The morphology of the region has been affected in the past by geological events such as the 9.2 magnitude earthquakes of 1964 (the most powerful earthquake recorded in North America) which moved land areas by a few meters; associated tsunami caused severe damage in Prince William Sound nearby. Large regions around Anchorage and Cook Inlet have not been mapped and are not accessible to direct observations. For example, the topographies of hundreds square kilometers of mudflats are largely unknown, though there are evidences that the morphology has been changed by the earthquake and continuous sediment movement.

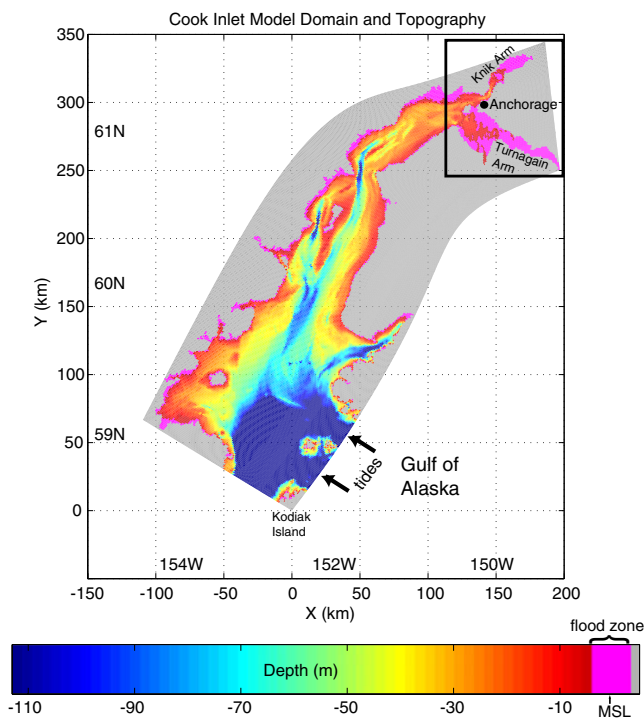


**Fig. 1** The CI model domain and topography (see Oey et al. 2007, for details). The depth (blue to red colors) is relative to the local mean sea level; gray areas are always dry land while magenta areas are inundation regions that can be wet or dry. Tidal forcing applied at the open boundaries on both sides of Kodiak Island. The area of interest of this study is the boxed region in the upper inlet

An inundation model has been developed for CI (Oey et al. 2007; Ezer et al. 2008), but its flood prediction capability is limited by a lack of accurate topography data for setting up the model and by a lack of observations of water coverage to validate the model. For example, Ezer and Liu (2009) compared the topography data currently available for the CI inundation model (Oey et al. 2007) with Landsat remote sensing data, demonstrating the much greater details that the remote sensing data can provide. So how can one use remote sensing data to study morphology and climatic changes, as well as improve flood prediction models? The idea is to use geographic information system (GIS) tools to combine numerical inundation models with remote sensing data. Preliminary feasibility studies (Oey et al. 2007; Ezer and Liu 2009; Liu and Ezer 2009), using Landsat and moderate resolution imaging spectroradiometer (MODIS) data demonstrate that the moving shorelines due to the tidal ebbing and flooding cycle can be inferred from satellite data. While satellite data such as Landsat can identify flooded/exposed mudflats regions and provide a two-dimensional picture of the water coverage, to describe the three-dimensional structure of the flooded zone, one needs to take into account the water level elevation (or sea surface height, SSH). In CI, at particular times in the tidal cycle, water level may change by as much as  $\sim 10$  m over  $\sim 50$  km distance (Oey et al. 2007). The spatial water level changes has not been addressed in the previous studies of remote sensing data (Ezer and Liu 2009; Liu and Ezer 2009), thus the need to integrate the satellite data with the inundation model.

The goal of the study is to develop the methodology to combine remote sensing data, sea-level observations and dynamic models in order to study the short- and long-term environmental impact of flooding and morphological changes. Eventually, the new analysis can also be used to evaluate and improve inundation models used for flood prediction in other regions.

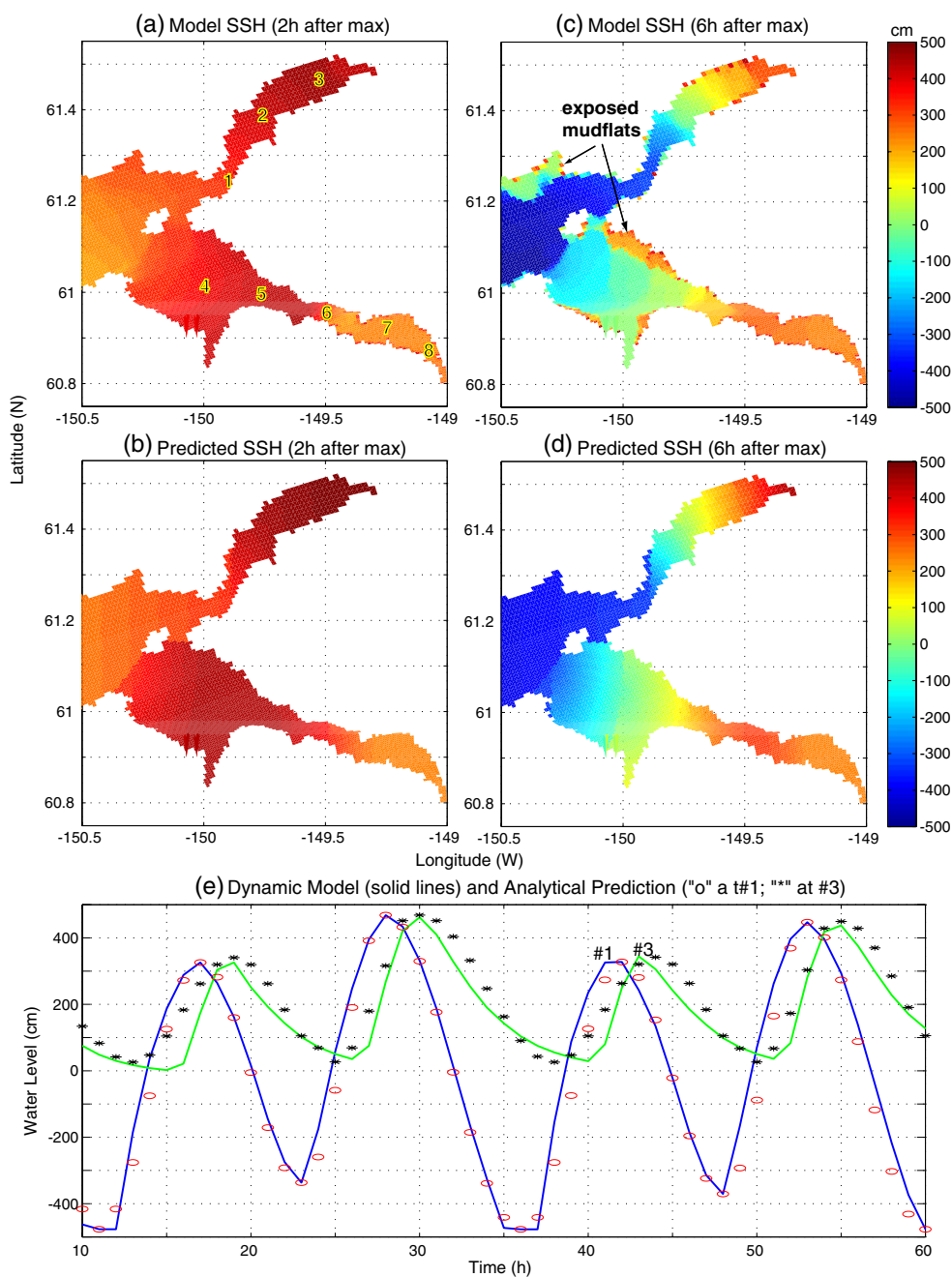
The paper is organized as follows. First in Section 2, the CI inundation model and the statistical flood prediction method are described and then in Section 3, the remote sensing analysis is described. The results of merging the satellite-derived data with the water level prediction are presented in Section 4, and discussions and conclusions are offered in Section 5.

## 2 Inundation modeling and water level prediction

### 2.1 The Cook Inlet numerical model

Inundation modeling referred to ocean models that include wetting and drying (WAD) algorithms that allow a movable land-water boundary. Unlike most oceanic general circulation

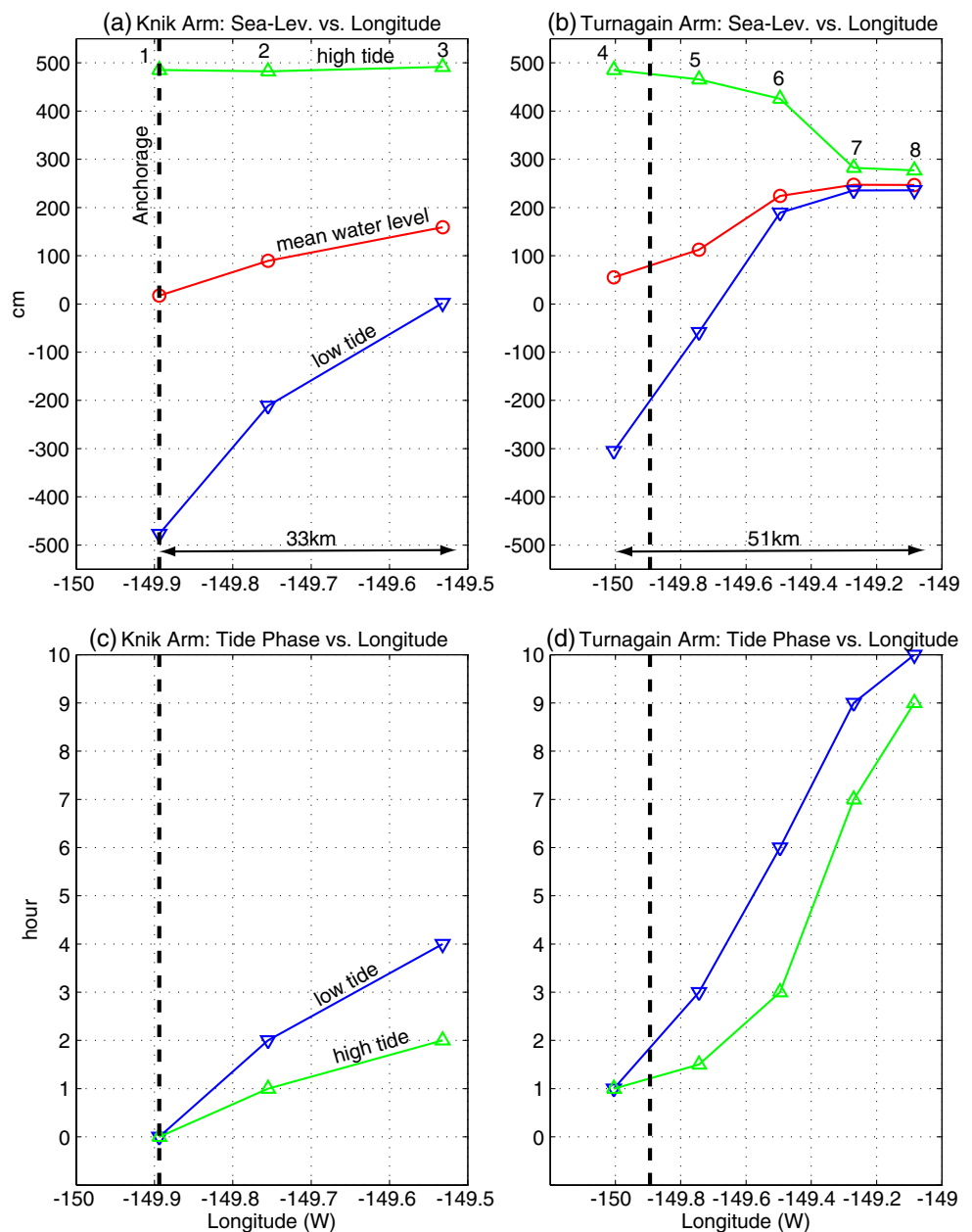
**Fig. 2** Comparison of the analytical water level (WL) prediction (Eq. 1) with the sea surface height (SSH) of the full three-dimensional numerical model. The numerical model results for **a** high tide and **c** low tide are compared with the analytical predictions in **b** and **d**, respectively. **e** Hourly time evolution of the predicted WL (open circle and asterisk) are compared with the model SSH for Anchorage (point #1 in **a**; blue line) and for the upper Knik Arm (point #3 in **a**; green line)



models that have a wall-like fixed coastal boundary, models with WAD can simulate flooding of land areas or exposing of shallow water-covered areas. In bays and inlets with large-amplitude tides, such as in the Bay of Fundy (Gulf of Maine) and the Cook Inlet (Alaska), WAD is an essential part of the local environment and ecosystem. In other places, inundations due to catastrophic events such as tsunamis or hurricane storm surges alter the shoreline and the ecosystem. Until recently WAD schemes have been implemented mostly in hydraulic and in coastal engineering models, but now such schemes are being implemented also in three-dimensional general circulation ocean models. We will use the inundation model recently

developed by Oey (2005, 2006), which was based on the community Princeton Ocean Model (i.e., version POM-WAD). Oey (2005, 2006) tested the inundation model for various 1D, 2D, and 3D idealized problems; see also Saramul and Ezer (2010) and Xue and Du (2010), for recent evaluation of the inundation processes in the model and their effect on mixing. The implementation of POM-WAD for the Cook Inlet (CI), Alaska, is described in Oey et al. (2007) and Ezer et al. (2008). The (predominantly semi-diurnal  $M_2$ ) tide entering from the Gulf of Alaska is amplified in CI, reaching an approximately 10-m range near Anchorage, and flooding hundreds of square kilometers of mudflats in the upper inlet.

**Fig. 3** The range of the amplitude (*upper panels*) and relative phase (*lower panels*) of the tides in Knik (*left*) and Turnagain (*right*) Arms for the eight locations indicated in Fig. 2a. Green, red, and blue lines represent the high, mean and low tides, respectively. The dashed vertical line is the location of the Anchorage tide gauge station



Therefore, CI can be served as an idealized natural lab to test and validate flood models. The CI model has been used to simulate tidal bores, rip tides, and the impact of river runoffs and other parameters (Oey et al. 2007). The same model has been also used to show that the movements of the endangered beluga whales up and down the inlet are synchronized with the tides (Ezer et al. 2008).

The main obstacle of getting accurate flood prediction in CI and elsewhere (say during hurricane storm surge) is the lack of detailed and up to date bottom topography data from deep waters to the land regions that potentially can be flooded. In the CI case, the best topography data was a  $1 \times 1$  km data obtained from the Woods Hole Oceanographic

Institute; this data set excluded the entire mudflat regions. Hand-charted data from NOAA's nautical charts (sounding data) provided the model with only rough estimates of the extents of the mudflats, but no details on the topography of the mudflats are available, due to the inaccessibility of the upper inlet to boaters. The derived model topography is shown in Fig. 1. There are 16 vertical layers (bottom-following, "sigma grid") and  $401 \times 151$  horizontal grid points in the model; grid size varies from  $\sim 1$  km near the Gulf of Alaska to less than 0.5 km in the upper inlet near Anchorage, where the inlet splits into the Knik and Turnagain Arms. The model includes the incoming tides from the Gulf of Alaska, winds, river runoffs, temperature,

and salinity, etc. The simulations show the complex nature of the dynamics, with tidal ranges that are amplified from 1–2 m in the southwest to 8–12 m in the upper inlet near Anchorage. The dynamics of the shallow arms is very non-linear- it may take a few hours for tidal bores to propagate and flood the far shallow ends of the inlet- by that time the ebb has already started near Anchorage. More details about the model can be found in Oey et al. (2007) and Ezer et al. (2008).

### 2.2 The water level prediction method

Only one tide gauge station is available in the upper CI, near Anchorage, and there are no direct observations of water coverage and water levels over the extensive

mudflats. To be able to study the huge spatial and temporal variations in CI water levels one has to take into account the delay in the propagation of the flood from the observed location at Anchorage toward the far end of the inlet. Our goal is to combine the water level with the shoreline analysis obtained from the satellite images (see next section). One way to do that is to run the inundation model for every period when remote sensing data is obtained and interpolate the model fields from the model grid points into each of the remote sensing pixels. This will require tremendous amount of work and computations. Therefore, we developed a simpler method to predict water level  $\eta^{\text{mod}}(x,y,t)$  at every point in the upper CI ( $x,y$  are longitude and latitude) and every time ( $t$ ) using the model statistics

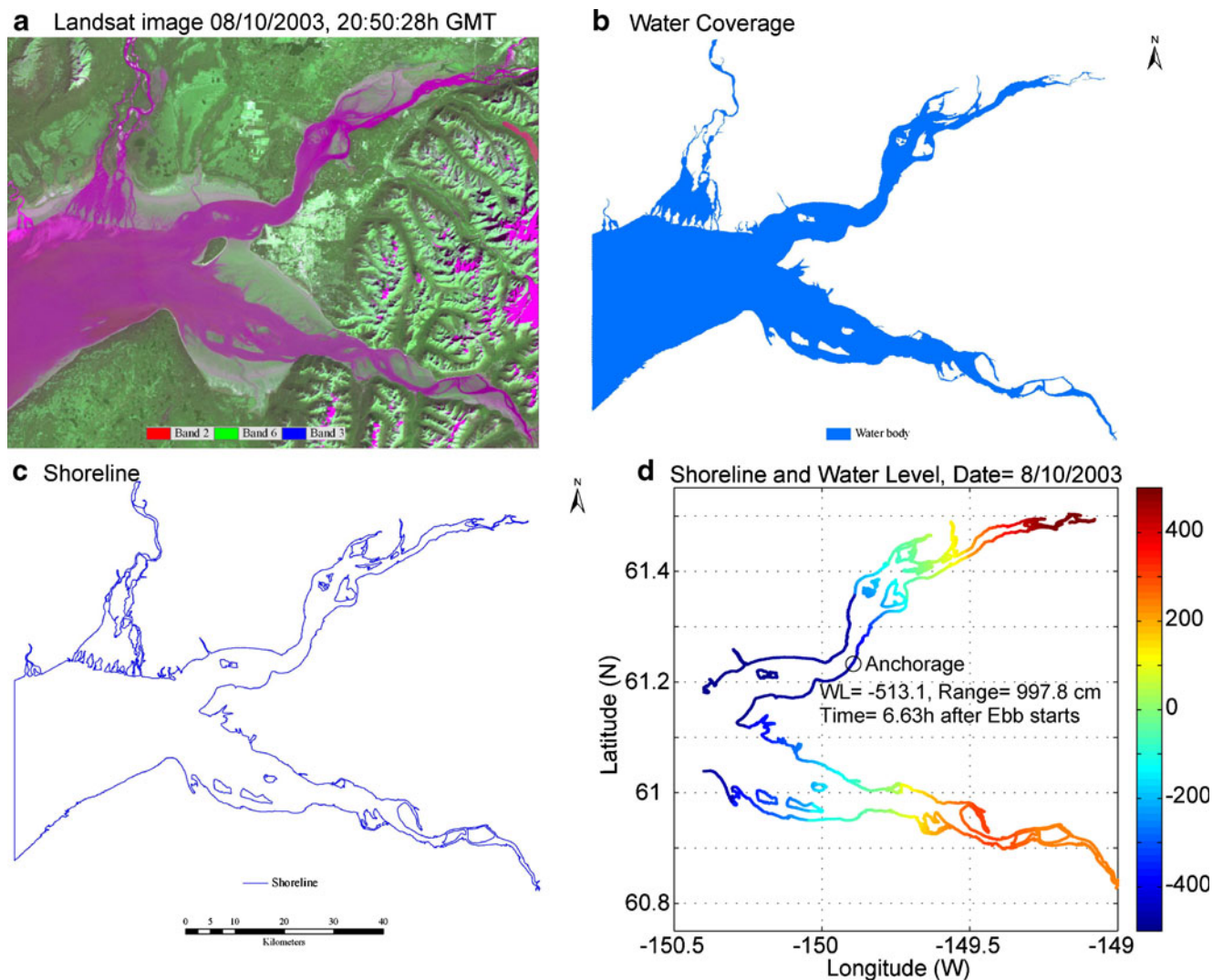


**Fig. 4** An example of the remote sensing data processing stages using a Landsat TM image acquired on 08/10/2003, 20:50 (GMT). **a** In the first stage, images with no clouds or ice are obtained and then pixels are classified to identify water or land areas. **b** In the second step, a water-only image is created from **a**. **c** In the third step, the boundary of the

water coverage area is derived from **b** and then the coordinates for the shoreline pixels are sampled at 30 m intervals and archived. Finally, the water level at Anchorage is obtained from NOAA for the time of each image and using the prediction procedure described in the text, the water level along the shores in **c** are calculated and shown (by color) in **d**

and the observed water level at Anchorage,  $\eta^{\text{obs}}(t)$ . The method includes the following steps:

- (1) From a long-term model sea-level calculation that covers many tidal cycles (say 1 year) a statistical correlation between water level (WL) at Anchorage and selected locations (Fig. 2a) are found. In particular, the mean high and low WL and the time delay ( $dt$ ) relative to Anchorage are calculated (Fig. 3). Note that away from Anchorage the tides are asymmetric (Fig. 2e) with shorter delay for high tides and longer for low tides, i.e., drainage during ebb is much slower than water surge during flood. It also takes several hours longer for the tide to reach the far end of Turnagain Arm (Fig. 3d), which is shallow and flat, than the far end of Knik Arm (Fig. 3c). The easternmost part of Turnagain Arm is very shallow ( $H \sim 1$  m) with small WL range (Fig. 3b), so shallow water waves, with speed of  $c=(gH)^{1/2}$  propagate much slower than in the deeper Knik Arm.
- (2) Now from the statistics above (Fig. 3), an empirical formula can be used to extrapolate from the observed WL in Anchorage to the rest of the upper inlet. The empirical formula we used for the predicted WL is of the form:

$$\eta^{\text{pred}}(x, y, t) = \eta^{\text{obs}}(t)A(x, y) \cos\{[2\pi/T][t - dt(x, y)]\} + B(x, y) \quad (1)$$

where  $\eta^{\text{obs}}(t)$  is the observed WL in Anchorage at time  $t$ ,  $T$  is tidal period (12.42 h for  $M_2$ ),  $dt(x, y)$  is the phase delay at location  $(x, y)$  relative to Anchorage,  $A(x, y)$ , and  $B(x, y)$  are the amplitude amplification factor and mean WL bias, respectively, at point  $(x, y)$  relative to Anchorage.  $A$ ,  $B$  and  $dt$  are empirical coefficients derived from the model statistics (Fig. 3). Note that because of the different dynamics in Knik and Turnagain Arms, Eq. 1 uses different values of

coefficients for each Arm. How well does the empirical formula work relative to calculations with the full numerical model? Fig. 2 demonstrates that this water level prediction is quite accurate, capturing for example the asymmetry of the tides (shorter flood and longer ebb). Overall, when compared with the dynamic calculations of the full three-dimensional model, errors are estimated to be  $\sim 10$ – $15\%$  of the tidal range. We are aware of course that the empirical coefficients in Eq. 1 are based on an imperfect model with an imperfect topography. In the future, one can improve the model topography with the method described below, then run a new model (with higher resolution), recalculate the coefficients and then recalculate even better topography. This iterative process is beyond the scope of this study, though we may try in the future to apply our WL prediction method to new high-resolution operational models now under early stages of development.

- (3) Using the method described above, for any given waterline location  $(x, y)$  and satellite time  $(t)$ , the WL can be analytically calculated. Besides the empirical coefficients, the only required input information for each image time are Anchorage WL,  $\eta^{\text{obs}}(t)$ , and tide amplitude (so Spring and Neap tides are considered in the amplification factor). The empirical coefficients are linearly interpolated from the points in Fig. 2a to each latitude–longitude location of the satellite analysis.

### 3 Remote sensing data and shoreline analysis

Remote sensing and GIS have been used extensively in monitoring water resources, for example, to assess water clarity of lakes in Minnesota using Landsat (Olmanson et al. 2008).

**Table 1** An example of the information collected for the remote sensing data over Cook Inlet, AK; here shown is the information for the images used in Fig. 5

Landsat acquisition data/time (GMT)	Cloud cover (%)	Anchorage tide (m)	Anchorage tidal stage	Wind speed (m/s)	Air temp (°C)	Water temp (°C)
2003/03/11, 21:02:19	18	2.201	00:08 h after high tide	2.000	−6.300	−0.900
2001/06/25, 21:02:56	18	1.237	02:26 h after high tide	2.100	15.600	14.700
2003/09/11, 20:51:03	10	−2.007	04:27 h after high tide	2.400	14.300	12.700
2003/08/10, 20:50:28	0	−5.131	00:58 h before low tide	2.500	17.000	15.300
2001/06/02, 20:57:20	9	−3.768	01:03 h after low tide	0.100	15.800	11.100
2002/10/02, 21:01:18	13	−1.875	02:01 h after low tide	1.000	9.500	8.800
2000/08/09, 21:04:39	7	−0.761	02:34 h after low tide	0.100	16.500	13.100
2002/05/20, 20:56:06	0	1.889	04:08 h after low tide	1.700	0.000	7.100

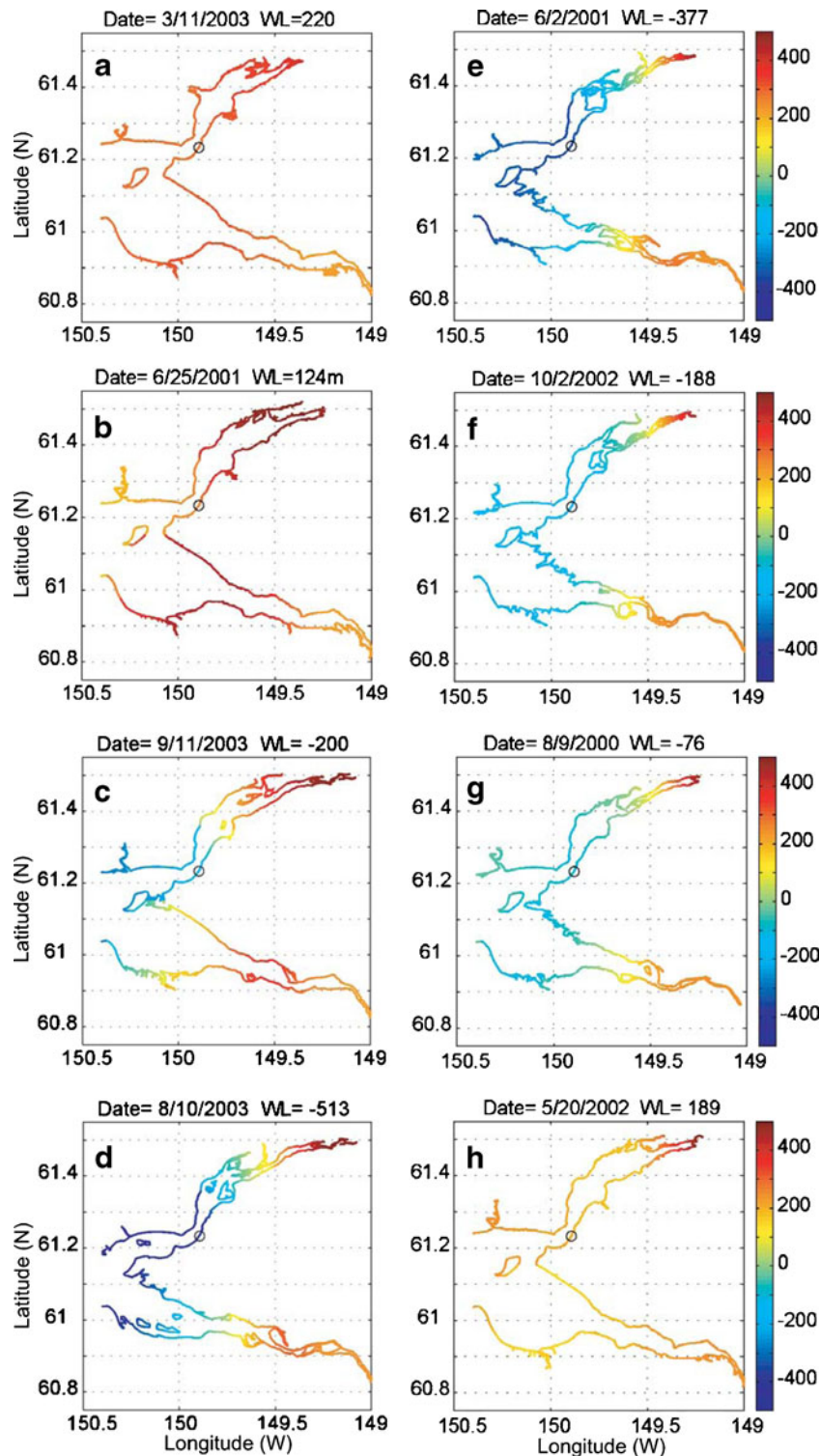


**Fig. 5** Shorelines and water levels (in cm) for a complete tidal cycle, during ebb (*left panels*) and flood (*right panels*). The water level at Anchorage is indicated for each image. The time intervals (in hours) from the beginning of ebb are: **a** 0.1, **b** 2.4, **c** 4.5, **d** 6.6, **e** 7.3, **f** 8.2, **g** 8.8, **h** 10.3

MODIS data were applied, for example, to monitor red tide in southwestern Florida coastal waters (Hu et al. 2005). Satellite data from Landsat, MODIS, and SPOT imagery can also be used to map shoreline changes caused by tides, storm surge

floods, tsunamis and other morphological processes caused by natural climatic changes (e.g., sea-level rise) or shore developments. The focus here is on the tidal-driven moving shorelines in CI. The idea of using MODIS data

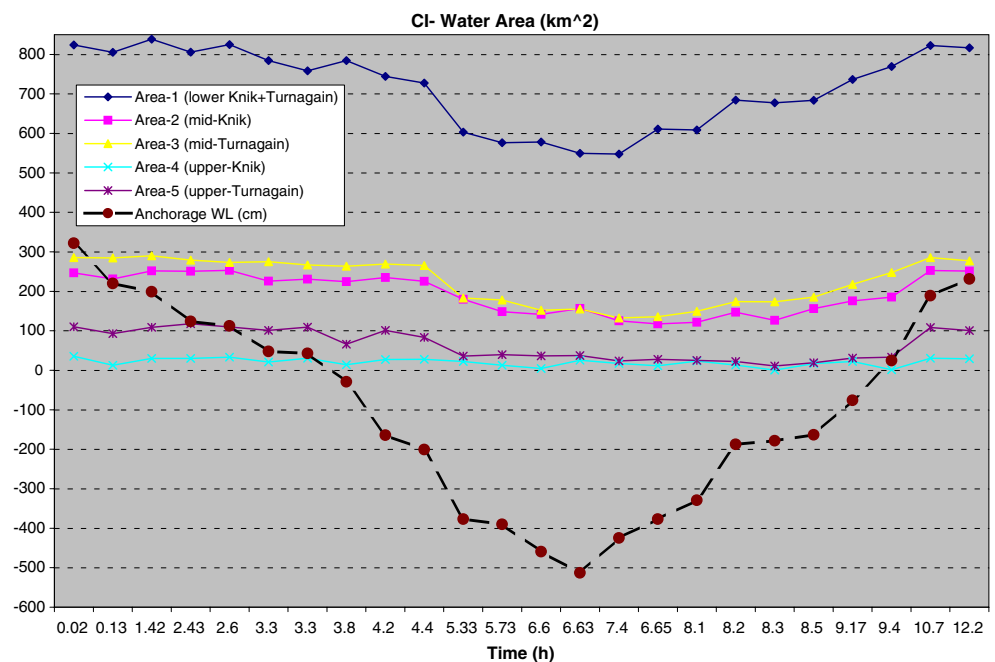
to improve model inundation predictions has been originally mentioned by Oey et al. (2007), but the relatively low spatial resolution of MODIS (250–500 m), may not be sufficient for mapping the details of the mudflats (Ezer and Liu 2009), so the higher resolution Landsat imagery (30–60 m) will be used here. Note that much higher resolution (and more expensive to obtain) LiDAR data are often used for water coverage studies (Bales et al. 2007; Zhou 2009), but these data are not available in most of the CI area; we will however, compare in the future our Landsat (free data) analysis with high-resolution Earth Observing SPOT (Stroppiana et al. 2002) data, a commercial product.

It is important to find reliable images (with minimal cloud cover or ice) at different tidal stages so the water coverage is different in each image. Figure 4a is an example of a Landsat image with Anchorage water level close to its lowest point, showing the expansion of water coverage; it also demonstrates the difficulty of discriminating between water and land in this complex-topography region. Note that at this high latitude only ice-free summer images can be used. Landsat Thematic Mapper (TM) and Enhanced Thematic Mapper Plus (ETM+) images can be downloaded from USGS GloVis (<http://glovis.usgs.gov/>). Both Landsat and SPOT sensors produce multispectral images with median to high spatial resolution (Landsat TM and ETM+ visible bands at 30 m resolution, SPOT-5 visible bands at 5–10 m resolution). In our experimental study here we show results obtained from some 25 Landsat images with acquisition date from 1983 to 2009 (more

images will be added in the future). Table 1 is an example of record that we have created to manage our remote sensing imagery. For each image we collected local data from the NOAA/NOS Anchorage station at the exact time the image was taken; as described above, the sea-level information is used in the water level predictions scheme (1). The atmospheric and water data may help us in future climate studies and identifying environmental conditions in cases of suspicious images (say potential ice or storm conditions).

Figure 4 demonstrates the steps taken in the analysis. First, the water coverage is identified from each image by classifying each pixel as land cover, water or wet mudflat. The accuracy of the image classification will be assessed and refined later by using SPOT and other data, to aim for total accuracy of at least 90%. Color aerial photos of Anchorage obtained from Geographic Information Network of Alaska are also used as references in image classification. The result of the first step is a series of water-only images (Fig. 4b). Next, the shorelines for each image are obtained from the boundary of the water pixels (Fig. 4c) and re-sampled at a resolution of 30 m (this will make it easier later to compare shorelines obtained from different sources with different image resolution). The last step (Fig. 4d) is to calculate the WL along the shorelines, using the observed WL in Anchorage at the time of each image and the prediction formula 1. The result of the above analysis is a set of shoreline data (~50,000 points per image) and associated water levels (represented by the color in Fig. 4d).

**Fig. 6** The observed Anchorage water level (dashed line and circles, in cm) and water-covered area (solid lines, in km<sup>2</sup>) for five sub-regions: (1) lower Knik and Turnagain Arms (150–150.5°W), (2) and (3) mid Arms (149.5–150°W) for Knik and Turnagain, respectively, (4) and (5) upper Arms (149–149.5°W) for Knik and Turnagain, respectively. The 24 images used are arranged in the order of their time relative to the start of ebb (x axis)



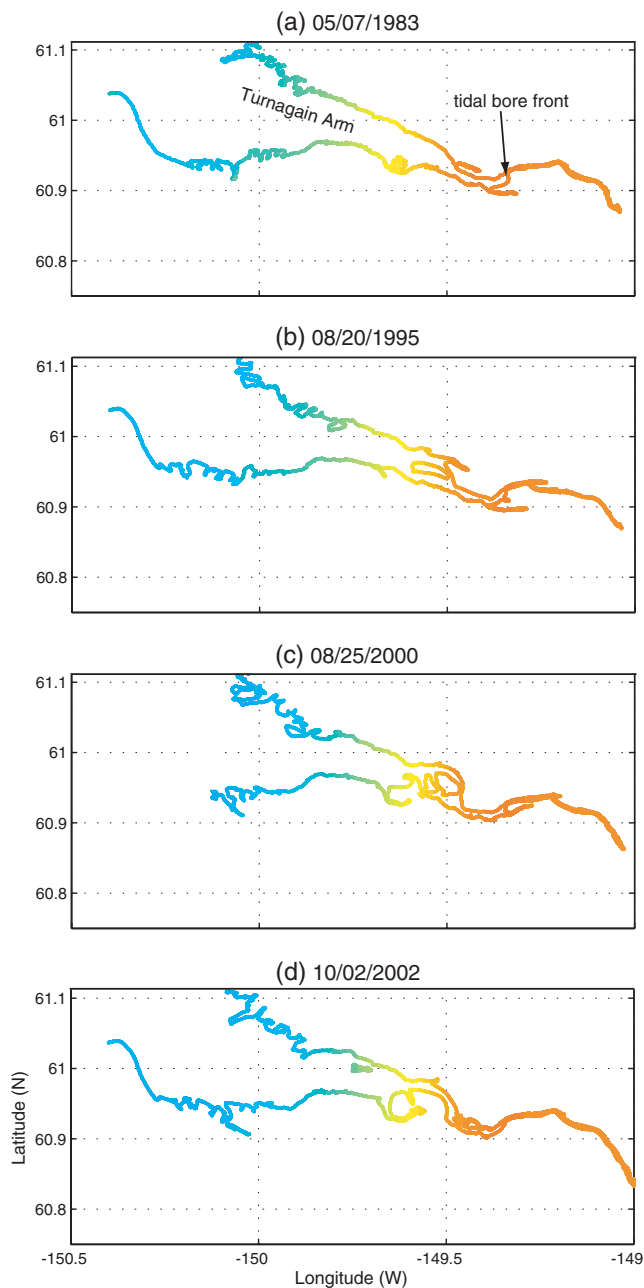


**Fig. 7** Comparison of the morphology of the mudflats in Turnagain Arm obtained from images taken from 1983 to 2002. The shorelines and WL (color) are as in Fig. 5. The four images used are all taken about 2 h after minimum WL was observed in Anchorage; the WL in Anchorage at that time is about 1.5 m below mean WL and rising (flood). Some data were missing in 2000 due to clouds

**4 Results: applications of the combined remote sensing and inundation analysis**

The analysis that combines the remote sensing of water coverage and shoreline detection with simulations of water level and inundation provides a new data set that can be used for various interdisciplinary studies. Considering that previously only about half of the upper CI had sounding

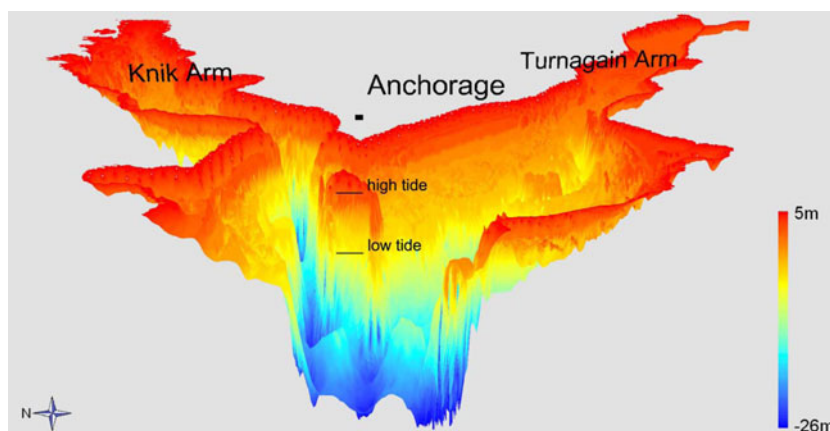
data of water depth (with no data over most mudflat areas), our analysis (even with the limited number of images shown here) provides over a million data points of shoreline locations and their water levels over almost three decades. Below are examples of potential applications of this data set.

**4.1 Dynamics of the inundation process during a tidal cycle**

The large tides are by far the dominant forcing in CI; winds and rivers play some role in the flow dynamics (e.g., rip tides in the mid and lower inlet), but have relatively small effect on the daily inundation in the upper inlet (Oey et al. 2007). If we also neglect potential long-term climatic changes (see the next section) one can consider a “typical” tidal cycle by looking at water coverage and shoreline obtained at different stages of the tidal cycle (though may be at different years). Figure 5 shows the moving shorelines and WL during one tidal cycle from satellite images taken between the years 2000 and 2003 (so potential long-term changes should be small). One should keep in mind that at any particular time variations in WL at different locations can be as large as 10 m, so when we refer to tidal stage (say, ebb or flood) we mean that at Anchorage. During ebb (Fig. 5a–d) Knik Arm is experiencing the receding waters first while Turnagain Arm with its shallow and flat end is not completely dry until a few hours after the flood began (Fig. 5f). During the lowest tide (Fig. 5d) several underwater “islands” are exposed, and Fire Island becomes connected to Anchorage (as known to local adventurers who try to make this 7-mile round trip before the tide returns). The front of the tidal bore in Turnagain Arm can be seen filling the Arm and propagating from ~149.7 W (Fig. 5e) to ~149.3 W (Fig. 5g) and to the end of the Arm, ~149.1 W (Fig. 5h), within ~3 h. This translates to a speed of  $c \sim 3 \text{ m s}^{-1}$ , close to that observed and modeled (Oey et al. 2007, simulated speeds of  $\sim 3\text{--}5 \text{ m s}^{-1}$ ). Such speed is consistent with the propagation of shallow gravity waves at the average depth of  $\sim 1 \text{ m}$ , i.e.,  $c=(gH)^{1/2}$ . Note that the maximum WL may reach the end of the Arm a few hours after the tidal bore; this, and the lack of accurate topography data for the uppermost part of the Arms in the model could explain why the time delay of the maximum seen in Fig. 3d is longer (~6 h).

The remote sensing analysis can also quantify the inundated area of the mudflats (Fig. 6). The change in the water-covered area of the lower Arms (by almost 300 km<sup>2</sup>, Area-1 in Fig. 6) is generally in phase with the Anchorage WL, though with slower draining than flooding, as mentioned before. The pattern of water coverage in the middle and upper Arms is quite different than the Anchorage WL (Areas 2–5 in Fig. 6), with a long period of exposed mudflats (~5 h) that lasts several hours after the flood have started.

**Fig. 8** Three-dimensional image of the average topography of CI obtained by composing together shorelines obtained from analysis of 25 Landsat images for inundated areas with the model topography of deeper regions



#### 4.2 Long-term morphological changes of the mudflats

Landsat satellites have been taking images of earth since the 1970s, so it is a useful tool to study climatic changes in land (e.g., Vogelmann et al. 2009) and in marine habitat (Palandro et al. 2008). Because of the strong tidal currents in CI, the morphology of the mudflats may change over time, though there are no direct observations of those changes. Figure 7 shows a comparison of the shoreline and WL obtained from four images covering almost 20 years (from mid 1983 to late 2002). All images were taken about 2 h after flooding began, when the tidal bore front is in the upper Turnagain Arm around 149.3°W. Changes of the morphology over time are clearly seen around 149.4°W–149.7°W. For example, between 1983 and 1995, the surging tide took a path through channels in the southern part of the Arm, but around 2000, a northern path started developing, and by 2002 all the water flow through the northern channel (a new southern channel farther west, around 149.7°W, seems to start also). Figure 7 is only an example that demonstrates the usefulness of our analysis for studies of the long-term changes, and more such comparisons are clearly envisioned in the future. One environmental application for this analysis would be to study whether the stranding of beluga whales (Vos and Shelden 2005) may relate to “danger zones” created by the rapid changes of the mudflats due to sediment transports.

#### 4.3 Improving the bathymetry of inundated coastlines

As mentioned before, there are no direct observations of the topography of the mudflats. The NOAA navigation charts, used to construct the model topography, lack any sounding data in the mudflats areas which are inaccessible and dangerous for boating. Can the remote sensing data give us a better estimate of the mudflat topography?

To demonstrate this possibility we composed together the information from some 25 analyses (similar to those shown in Figs. 5 and 7) each has about 50,000 to 80,000  $(x,y,H)$  points, they represent over a million shoreline “observations”. In each 50×50-m box, the average depth (relative to mean WL in Anchorage) is calculated. This calculation represents the “mean” topography of all the inundated area (neglecting morphological changes as discussed in section 4.2). For regions that are always covered with water we use the model topography (which is based on a 1×1-km topography data base obtained from WHOI). Figure 8 shows the estimated three-dimensional topography obtained this way. It shows for example a “seamount” in the lower Turnagain Arm that was missing from the original model topography. More refinement is clearly needed, especially in the very shallow regions, using more images and possibly combining the remote sensing analysis of inundated regions with high-resolution land elevation data. Another usage may be to create separate topographies for different periods (say, decades) in order to study climatic changes. Here, we only demonstrate the basic approach with limited number of images.

#### 4.4 Providing data for evaluating and improving inundation modeling

The main motivation for this study came from the need to evaluate and improve the CI inundation model. Since no high-resolution data such as LiDAR were available for this region, publicly available (and free) remote sensing data from MODIS were first used qualitatively Oey et al. (2007), but Ezer and Liu (2009) showed that the spatial resolution of MODIS was insufficient to resolve the details of the mudflats topography, thus Landsat data may be a better choice (Liu and Ezer 2009). To construct a more accurate inundation model with higher resolution would not be

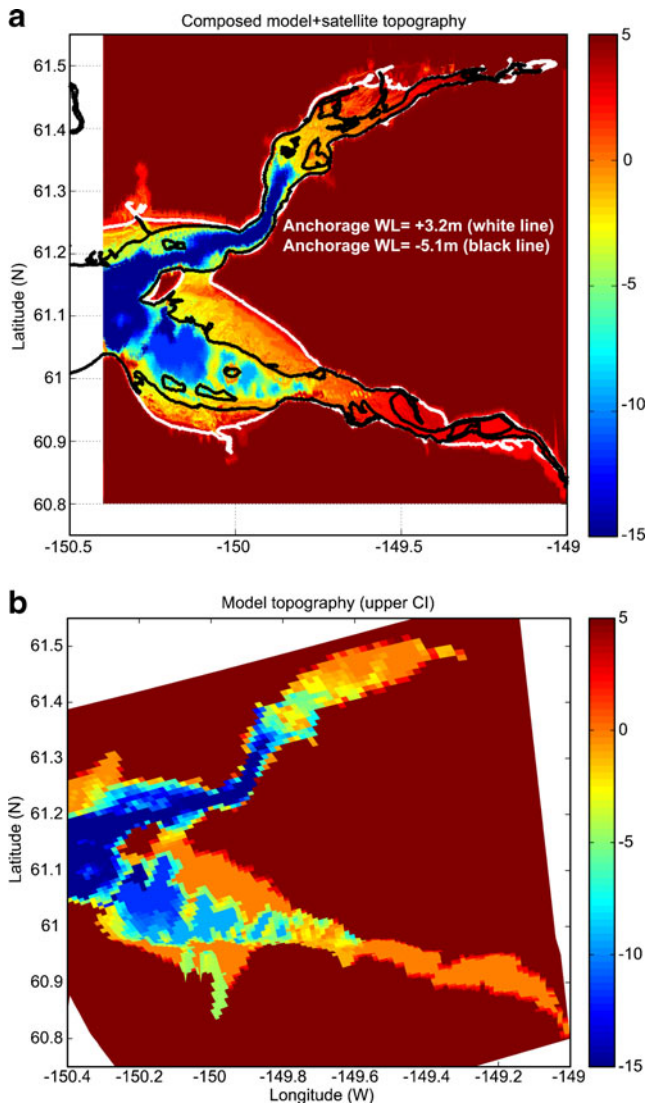


**Fig. 9** The bottom topography (in m relative to local MSL) from **a** the composed analysis of the remote sensing data and the model, and **b** from the model grid alone. In **a** the shorelines during low tide (10-Aug-2003) and high tide (11-Mar-2003) are shown in *black* and *white* lines, respectively

possible without much more accurate and detailed topography; one way to improve the model topography is using remote sensing data as suggested here. Figure 9 shows a comparison between the model topography and the new “mean” topography obtained from our remote sensing analysis. It is clear that while the basic shapes of the topography in the model is correct, it lacks the details of some features, such as the underwater “seamounts” seen around 150.1°W, 61°N and around 150.2°W, 61.22°N. The narrow channels in the westernmost part of Turnagain Arm with size of tens of meters seen in the Landsat data cannot be resolved in the model with ~500 m resolution. Further refinement of our analysis with additional satellite images would allow us to

construct a new high-resolution model with more accurate topography, then, one can evaluate the WL prediction (1) and if needed, further improve the topography analysis. However, at this point, there are no independent observations over the mudflats to evaluate the model.

### 5 Summary and conclusions

The idea of using MODIS data to identify water coverage and evaluate flood prediction of inundation models has been first demonstrated qualitatively in Oey et al. (2007). However, the spatial resolution of MODIS (250–500 m) is probably insufficient for the complex mudflat topography in CI, as demonstrated by Ezer and Liu (2009) who compared the MODIS data with higher resolution Landsat data (30–60 m). However, the infrequent temporal resolution of Landsat and other high spatial resolution remote sensing instruments (compared with the 12-h tidal cycle in the study area) require acquiring images over a long period of time to have large data set with images capturing many different stages of flooding. Note that at this high latitude, only ice-free summer images can be used for mapping the shoreline; images with partial ice cover can be used, however, to study long-term climate changes that may affect the ice-covered area.

The analysis method described here involves classification of Landsat images into three categories: water, mudflat, and others (land) and derivation of water coverage and shoreline coordinates for each of many images collected since the 1980s. Because of the large spatial WL changes in CI (~10 m over ~50 km distance) for each time an image is available, the WL distribution is estimated from the statistics of the inundation model. This WL prediction method extrapolates WL from the only observed station in Anchorage to the entire upper Inlet, taking into account the long delay (several hours) in tidal phase between the shallow part of the two CI Arms and Anchorage. The result is a new data set of shorelines position and WL covering the inundated mudflat regions over many years. Several applications of this analysis have been demonstrated:

1. Composing all the images together can be used to derive a best estimate long-term mean topography  $H(x,y)$  of the upper inlet. Even in our example of limited number of images (~25), the combined data set includes over million data points, which is many orders of magnitude more data than was previously available from sounding data.
2. These data can be the base for constructing an improved inundation model with much higher resolution than previously was possible (say, 10–50-m grid size instead of 500 m). It is very clear that the topography that was

available when the model was constructed was quite inaccurate in the uppermost parts of CI where direct observations were not available, so the WL prediction method (1) should be retested with the new model.

3. The analysis can help study morphological changes of mudflat topography. Such changes can result from sediment transport by the strong tidal currents, man-made shore development or geological events (e.g., the 9.2-magnitude “Good Friday earthquakes” of 1964 has significantly changed the topography of some regions in CI). It was demonstrated here that our analysis was able to show significant changes in the morphology over a period of ~20 years, as a result the surging tides change their path or create new channels. One can extend the analysis with additional data to derive a composite topography for different periods, say for each decade, and compare changes in morphology and urban environment and shoreline development over time.
4. The morphology maps will be also useful for our study of the movement and survival of the beluga whales (Ezer et al. 2008) and their adjustment to environmental changes. Other activity in CI such as the ongoing efforts to build tidal power stations, bridges and oil/gas explorations will benefit from the new data.

As part of the Alaska Ocean Observing System, there are currently attempts by NOAA and others to develop operational models for CI. The biggest obstacle for this effort seems to be the lack of data to represent the mudflats topography in the models and to evaluate the model inundation capability, so the method presented here may be one of the few ways to do that. The results presented here are a “proof of concept” demonstration of the methodology that combines remote sensing data with inundation models. Similar remote sensing analysis for other coastal regions and estuaries can be done. Further applications of our methodology include studies of floods associated with catastrophic events such as hurricane-driven storm surges and tsunamis, as well as impact of sea-level rise on various coasts.

## 6 Acknowledgments

The Cook Inlet inundation model was originally developed at Princeton University by L. Oey with support from the Mineral Management Service. ODU’s Office of Research provided funding to HL and TE through the Summer Experience Enhancing Collaborative Research (SEECR award). Additional support was provided to TE by NOAA’s National Marine Fisheries Service.

## References

- Bales J, Wagner CR, Tighe KC, Terziotti S (2007) LiDAR-derived flood-inundation maps for real-time flood mapping applications, Tar River, North Carolina. U.S. Geological Survey Scientific Investigations Report 2007-5032.
- Ezer T, Liu H (2009) Combining remote sensing data and inundation modeling to map tidal mudflat regions and improve flood predictions: a proof of concept demonstration in Cook Inlet, Alaska. *Geophys Res Lett* 36:L04605. doi:10.29/2008GL036873
- Ezer T, Hobbs R, Oey L-Y (2008) On the movement of beluga whales in Cook Inlet, Alaska: simulations of tidal and environmental impacts using a hydrodynamic inundation model. *Oceanography* 21(4):186–195
- Hu C, Muller-Karger FE, Taylor C, Carder KL, Kelble C, Johns E, Heil CA (2005) Red tide detection and tracing using MODIS fluorescence data: a regional example in SW Florida coastal waters. *Rem Sens Env* 97(3):311–321
- Liu H, Ezer T (2009) Integration of Landsat imagery and an inundation model in flood assessment and predictions: a case study in Cook Inlet, Alaska, The 17th International Conference on Geoinformatics, Fairfax, VA, August 12–14. IEEE Xplore Paper 209:1–5
- Kowalik Z, Knight W, Logan T, Whitmore P (2006) The tsunami of 26 December, 2004: numerical modeling and energy considerations. *Pure Appl Geophys* 164:1–15
- Oey L-Y (2005) A wetting and drying scheme for POM. *Ocean Model* 9:133–150
- Oey L-Y (2006) An OGCM with movable land-sea boundaries. *Ocean Model* 13:176–195
- Oey L-Y, Ezer T, Hu C, Muller-Karger FE (2007) Baroclinic tidal flows and inundation processes in Cook Inlet, Alaska: numerical modeling and satellite observations. *Ocean Dyn* 57:205–221. doi:10.1007/s10236-007-0103-8
- Olmanson LG, Bauer ME, Brezonik PL (2008) A 20-year Landsat water clarity census of Minnesota’s 10,000 lakes. *Remote Sens Envir* 112(11):4086–4097
- Palandro PA, Andréfouët S, Hu C, Hallock P, Müller-Karger FE, Dustan P, Callahan MK, Kranenburg C, Beaver CR (2008) Quantification of two decades of shallow-water coral reef habitat decline in the Florida Keys National Marine Sanctuary using Landsat data (1984–2002). *Rem Sens Env* 112(8):3388–3399
- Saramul S, Ezer T (2010) Tidal-driven dynamics and mixing processes in a coastal ocean model with wetting and drying. *Ocean Dyn* 60(2):461–478. doi:10.1007/s10236-009-0250-1
- Stroppiana D, Pinnock S, Pereira JMC, Gregoire JM (2002) Radiometric analysis of SPOT-VEGETATION images for burnt area detection in Northern Australia. *Rem Sens Env* 82:21–37
- Travis J (2005) Hurricane Katrina: scientists’ fears come true as hurricane floods New Orleans. *Science* 309(5741):1656–1659
- Vogelmann JE, Tolk B, Zhu Z (2009) Monitoring forest changes in the southwestern United States using multi-temporal Landsat data. *Rem Sens Env* 113(8):1739–1748
- Vos DJ, Shelden KEW (2005) Unusual mortality in the depleted Cook Inlet Beluga (*Delphinapterus leucas*) population. *North West Nat* 86(2):59–65
- Xue H, Du Y (2010) Implementation of a wetting-and-drying model in simulating the Kennebec–Androsoggin plume and the circulation in Casco Bay. *Ocean Dyn* 60(2):341–357
- Zhou G (2009) Coastal 3-D morphological change analysis using LiDAR series data: a case study of Assateague Island National Seashore. *J Coast Res* 25(2):435–447